PREDICTING WILDLAND FIRE BEHAVIOR AND EMISSIONS USING A FINE-SCALE PHYSICAL MODEL

B. Porterie , J. L. Consalvi , A. Kaiss & J. C. Loraud

Taylor & Francis
Taylor & Francis Group

PREDICTING WILDLAND FIRE BEHAVIOR AND EMISSIONS USING A FINE-SCALE PHYSICAL MODEL

B. Porterie, J. L. Consalvi, A. Kaiss and J. C. Loraud
Department of Mechanical Engineering, IUSTI CNRS, Technopôle de Château-Gombert, Marseille, France

A physical fine-scale two-phase model has been developed for the purpose of determining wildland fire behavior and emissions. The situation modeled corresponds to a spreading wildfire driven by wind through a fuel bed of combustible elements. The numerical model solves a set of time-dependent conservation equations for both phases (the gas and the vegetation elements) coupled through exchange terms. It accounts for the dynamics, turbulence, soot formation, and radiation. This model has been applied to a prescribed savanna fire. Good qualitative agreement was found between the simulation results and available in situ experimental data on the rate of spread and fuel consumption ratio.

1. INTRODUCTION

Wildfire is the manifestation of a chemical reaction between a combustible matter and oxygen from the air, the result of which is a release of energy and production of chemical species and soot. This chemical reaction, which occurs in the near-source region of the wildland fire, governs the fire's behavior at a larger scale and affects the near-ground layer of atmosphere. In return, the fire source is strongly affected by the surrounding atmospheric environment.

The main purpose of this work is twofold: to describe fire behavior and to determine the emissions of gaseous species and soot particles in the near-source region of the fire using a fine-scale two-phase field model. Small-scale models, such as that presented in this article, may be used to quantify the impact of wildfire emissions on nearby urban areas. They also may be coupled with atmospheric models to refine the description of the strong interactions between the fire and the atmosphere above the fire. This need has been expressed by Crutzen and Carmichael [1] and more recently by Trentmann et al. [2], who used the well-known atmospheric model ATHAM to simulate the atmospheric evolution of the plume from a prescribed biomass fire. In this simulation, "the fire is represented by heat and particulate fluxes in the lowest vertical model layer at prescribed grid boxes, and there is no feedback from the atmospheric wind field on the fluxes from the fire." The authors suggested that the temporal and spatial distributions of heat and particle emissions from the fire could be evaluated from a small-scale model. Concerning forest fuel combustion-product emissions, the contribution of the Russian school through the impetus given by A. M. Grishin is notable [3, 4].

NOMENCLATURE

a	absorption coefficient, m^{-1}.	u, v	x-, y- components of the velocity vector, m/s
A_k	specific wetted area of the solid phase $(= \alpha_k \sigma_k)$, m^{-1}.	w_m	weighting factor for a specific ordinate direction, m
C_p	specific heat of the gaseous mixture $(= \sum_\alpha Y_\alpha C_{p\alpha})$, $J/kg\,K$.	WWF	wet wildland fuel matter
DWF	dry wildland fuel matter	x, y	Cartesian coordinates
f_{v_s}	soot volume fraction	Y_α	mass fraction of species α
F_i	drag force component in the ith direction	α	phase volume fraction
g_i	gravity acceleration component in the ith direction	δ_{ij}	Kronecker delta
G	average incident radiation, W/m^2.	ε	dissipation rate of k, $m^2 s^3$
I	radiative intensity, $W/m^2\,sr$.	λ	thermal conductivity, $W/m\,K$
I_b	black-body radiative intensity $[I_b(T) = \sigma T^4/\pi]$, $W/m^2\,sr$	μ	viscosity, kg/m
h	enthalpy, J/kg	μ_m, ξ_m	direction cosines for a specific ordinate direction, m
Δh	heat of reaction, J/kg	ρ	density, kg/m^3
$\Delta h_{f\alpha}^0$	enthalpy of formation of species α, J/kg	σ	Stefan-Boltzmann constant, $W/m^2\,K^4$
k	turbulent energy, m^2/s^2	σ_k	surface area-to-volume ratio of a solid particle, m^{-1}
KNP	Kruger National Park		
L	latent heat, J/kg	σ_ϕ	turbulent Prandtl/Schmidt number for ϕ
m_k	mass of the solid phase per unit volume $(= \alpha_k \rho_k)$, $kg/m^3 s$	ϕ	any variable
$\dot{m}_k$	rate of mass lost by thermal degradation of the solid phase, $kg/m^3\,s^1$	$\dot{\omega}_\alpha$	rate of production of species α due to chemical reactions, $kg/m^3\,s$
p_g	pressure, Pa	Ω	directional vector of radiative intensity
Pr	Prandtl number $(= \mu_g C_p/\lambda_g)$	**Subscripts**	
q	heat flux vector, W/m^2	c	convective/conductive
Q	energy influx, W/m^3	g	gas phase
s, s_1	stoichiometric ratios for heterogeneous and homogeneous chemical reactions	k	particle phase k
		m	discrete direction
		r	radiative
		s	soot
T	temperature, K	α	species

From another point of view, the use of sensors in fire detection requires the calculation of radiation from the fire, which is the source of the signal received by the sensor. To perform this calculation, the temperature field in the fire zone (and near-atmosphere) is needed, along with the concentration of gases and the amount of smoke particles. Answering this question, the present model can be used to minimize some uncertainties linked to fire observation and characterization, for instance, by non-fire-dedicated sensors.

Our model is applied to experimental savanna fires in Kruger National Park (KNP) in Southern Africa in the frame of the South African Fire-Atmosphere Research Initiative (SAFARI-92). The significance of savanna fires is obvious. Andreae [5] estimated that the biomass burned every year over Africa is 390 million tons for forests and 2,430 million tons for savannas, which represents around half of the biomass burned worldwide. Moreover, savanna fires all have the distinctive feature of having a high rate of propagation, as the bulk density is low and the fuel

elements are thin. Very high propagation rates are possible under drought conditions, when fuel moisture content is low.

2.   WILDFIRE BEHAVIOR MODEL

Simple observations of the spread of wildland fires reveal that the bed may be separated into three areas as shown in Figure 1: the unburnt fuel, where heating, drying, and slow pyrolysis occur; the combustion zone, including intense pyrolysis and char combustion; and the burned residue.

The situation modeled corresponds to a wind-aided fire spread configuration. In a part of the combustion zone, the pyrolized fuel vapor leaves the fuel material, convects and diffuses outward, mixes with the oxidizer gas, and forms a combustible mixture ahead of the flame leading edge. Then this mixture is ignited by the flame. The generated flame can then be characterized as a free, turbulent, radiating, and sooty diffusion flame. Once all the pyrolyzates are depleted in the particle, flaming ceases. If oxygen is present, glowing combustion of the char occurs. The rate of fire spread can be expressed in terms of finding the translation rate of the ignition interface separating the burning zone and the unburnt fuel. It is therefore dependent on the ability of the flame and burning region of the fuel bed to supply a sufficient amount of heat to pyrolyze the fuel and to ignite the pyrolysis product/oxidizer mixture ahead of the flame. The heat transfer from the flame to the unburnt solid material is also strongly dependent on the flame outline, which in turn depends on the dynamic structure of the gas flow. In a wind-aided configuration, the flame is very close to the fuel bed during the heating, drying, and pyrolysis processes, which favors the heat transfer from the flame to the unburnt fuel. In a previous article [6], the influence of wind on the behavior of a line fire spreading through wildland fuels (pine needles) and the induced hydrodynamics inside and above the fuel bed were examined and showed fairly good comparison between computed and experimental results at a laboratory scale. The analysis of heat flux distributions at the top of the fuel bed confirms the conclusions of Pagni and Peterson [7] on the predominance of radiation for low convective velocities and that of convection with a significant
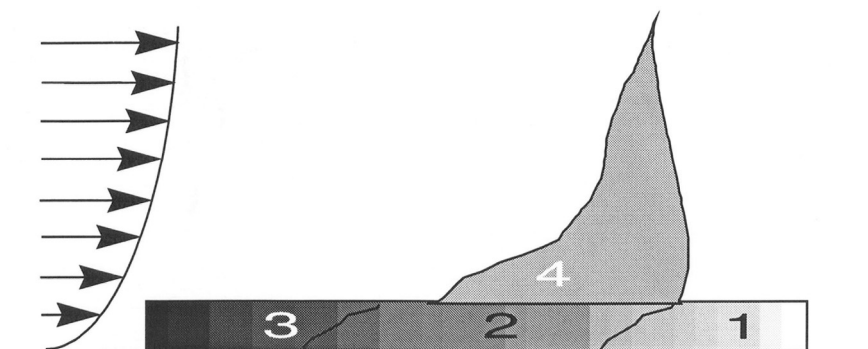

Figure 1. Structure of the fire front propagating through a fuel bed: 1, unburned heated fuel (drying, slow pyrolysis); 2, burning zone (intense pyrolysis, homogeneous and heterogeneous reactions, flameless smoldering combustion); 3, ashes; 4, turbulent luminous free flame.

radiative contribution for intermediate and high velocities. The ability of such physical two-phase model to effectively address the problem of firebreak efficiency [8] or to predict the onset of crowning [9] is illustrated.

In contrast to the well-known statistical and empirical models [10], the present model belongs to the class of physical models initiated by Grishin [11] (see also the monograh of Grishin published in [12] and also more recently [13]). This model accounts for each mechanism of heat transfer (conduction, convection, and radiation) individually. It describes the hydrodynamics through the fuel matrix and above the fuel bed, and incorporates first-order kinetics to describe drying, pyrolysis, and combustion. In this approach, a gas phase flows through a fuel bed which is viewed as an agglomeration of combustible, organic, and randomly oriented elements. For the present study, the fuel bed is considered as homogeneous, i.e., all particles have the same geometric and thermophysical properties and therefore belong to the same class of the solid phase. The gas and solid phase (the vegetation elements) in thermal nonequilibrium are assumed to be interdispersed and coupled by appropriate interaction terms. Each phase is treated as a continuum (Eulerian-Eulerian approach) and governed individually by a set of time-dependent equations. Then, any small volume in the domain of interest can be imagined as containing a volume fraction of each phase. The mathematical description of the physical problem is given below for a medium composed of a gas phase and a single-class solid phase $\left(\alpha_g + \alpha_k = 1\right)$; generalization to a multiclass solid phase can easily be obtained.

2.1. Analysis

2.1.1. Governing Equations. In the present numerical model, the gas phase is computed by solving the set of two-phase, turbulence-modeled, density-weighted, averaged conservation equations for mass, momentum, energy, and species, together with transport equations for the turbulence variables k and ε. The equation set is closed using the renormalization group theory (RNG) k–ε turbulence model [14] with additional buoyancy-driven production/destruction. The RNG k–ε turbulence model yields a more accurate prediction of the mean flow than the standard k–ε model for the treatment of nonequilibrium turbulence regions (separate flows and stagnation zones). It has been used successfully in both weak and fully developed turbulence regions.

The general form of the elliptic differential equations is given by

$$\frac{\partial}{\partial t}(\rho\phi) + \frac{\partial}{\partial x_j}\left(\rho\phi u_j\right) = \frac{\partial}{\partial x_j}\left(\Gamma_\phi \frac{\partial\phi}{\partial x_j}\right) + S_\phi \tag{1}$$

In Table 1, the source terms, S_ϕ, and the effective exchange coefficients, Γ_ϕ, are summarized for the different variables, and the constants of the turbulence model are listed. The additional soot transport equations that appear in this table will be discussed further.

The gas is assumed to be a mixture of perfect gases and, including the chemical energy in the mixture static enthalpy, the equations of state takes the form

$$p_g = \rho_g RT \sum_\alpha \frac{Y_\alpha}{W_\alpha} \tag{2}$$

Table 1. Sumary of the key equations expressed in the generic form. In this table, ϕ is the generic fluid property, Γ_ϕ and S_ϕ the exchange coefficients and source terms

Transport of	ϕ	Γ_ϕ	S_ϕ
Mass	1	0	S_m
Momentum	ui	μ_{eff}	$-\alpha_g \dfrac{\partial p_g}{\partial x_i}\rho g_i$ $+\dfrac{\partial}{\partial x_j}\left[\mu_{\text{eff}}\left(\dfrac{\partial u_i}{\partial x_j}+\dfrac{\partial u_i}{\partial x_i}\right)\right]$ $-\dfrac{\partial}{\partial x_j}\left[\dfrac{2}{3}\mu_{\text{eff}}\dfrac{\partial u_k}{\partial x_k}\delta_{ij}\right]-F_i$
Enthalpy	h	$\dfrac{\mu}{\text{PR}}+\dfrac{\mu_t}{\sigma_t}$	$-\dfrac{\partial q_{rj}}{\partial x_j}-Q_{rg}-Q_c+S_h$
Kinetic energy of turbulence	k	$\mu+\dfrac{\mu_t}{\sigma_k}$	$P+W-\rho\varepsilon$
Rate of dissipation of turbulent energy	ε	$\mu+\dfrac{\mu_t}{\sigma_\varepsilon}$	$(C_{\varepsilon1}-R)\dfrac{\varepsilon}{k}P-C_{\varepsilon2}\rho\dfrac{\varepsilon^2}{k}+C_{\varepsilon3}\dfrac{\varepsilon}{k}W$
SOOT volume fraction	f_{vs}	$\dfrac{\mu_t}{\sigma f}$	$-\dfrac{\partial}{\partial x_j}\left(0.55\mu\dfrac{1}{T}\dfrac{\partial T}{\partial x_j}f_{vs}\right)+\rho R_+ - \rho R_-$
Species mass fraction	Y_α	$\dfrac{\mu}{\text{Sc}}+\dfrac{\mu_t}{\sigma_f}$	$\dot{\omega}_\alpha+S_{Y_\alpha}$

where $\rho=\alpha_g\rho_g$, $\mu=\alpha_g\mu_g$, $\mu_t=\rho C_\mu\left(k^2/\varepsilon\right)$, and $\mu_{\text{eff}}=\mu+\mu_t$. The shear and buoyancy turbulent production/destruction terms P and W can be expressed by

$$P=-\left[\mu_t\left(\frac{\partial u_i}{\partial x_j}+\frac{\partial u_j}{\partial x_i}\right)-\frac{2}{3}\left(\mu_t\frac{\partial u_k}{\partial x_k}+\rho k\right)\delta_{ij}\right]\frac{\partial u_i}{\partial x_j}$$

$$W=-\beta g\frac{\mu t}{\sigma_t}\frac{\partial T}{\partial x_j}$$

with

$$R=\frac{\eta(1-\eta/\eta o)}{1+\beta\eta^3} \qquad \eta=\sqrt{\left|\frac{P_k}{\rho C_\mu\varepsilon}\right|}$$

$$\eta_o=4.38 \qquad \beta=0.015 \qquad C_\mu=0.0845 \qquad C_{\varepsilon1}=1.42$$

$$C_{\varepsilon2}=1.68 \qquad C_{\varepsilon3}=1.5 \qquad \sigma_k=0.7179$$

$$\sigma_\varepsilon=1.3 \qquad \sigma_f=\sigma_t=0.7 \qquad \text{Sc}=\text{Pr}=0.71$$

$$h=\sum_\alpha Y_\alpha\left[\Delta h_{f\alpha}^0+\int_{T_0}^T C_{p\alpha}(T)dT\right] \tag{3}$$

The specific heat and viscosity for each species of the gas phase are functions of temperature and composition.

The composition of pyrolysis products is complicated and depends on temperature, which explains the five-component limitation for the gas phase. Concerning combustion in the gas phase, the kinetic scheme is simplified by assuming that combustible pyrolysis products are an effective gas of the CO type [12]. The application

of a five-component simplified model was justified by Grishin in performing numerical resolutions of the problem of a thermal heat blast in a five-component (CO, O_2, CO_2, H_2O, and N_2) and seven-component (CO, CH_4, H_2, O_2, CO_2, H_2O, and N_2) combustible mixture. It was shown that the temperature deviations do not exceed 4%. In the present study, the major gas species which are taken into consideration are CO, O_2, CO_2, H_2O, and N_2. These species are identified by their mass fraction Y_α as follows: $Y_1 \rightarrow CO$, $Y_2 \rightarrow O_2$, $Y_3 \rightarrow CO_2$, $Y_4 \rightarrow H_2O$, $Y_5 \rightarrow N_2$.

So, the global oxidation reaction is simply $CO + \frac{1}{2}O_2 \rightarrow CO_2$ ($s_1 = 4/7$). Assuming fast reaction, the burning rate of carbon monoxide is limited by the turbulence dissipation rates of either fuel, oxygen, or hot products, the slower of which will control the local reaction rate [15],

$$\dot{\omega}_{CO} = -\rho \frac{\varepsilon}{k} \min\left(C_R Y_{CO}, C_R \frac{Y_{O_2}}{s_1}, \frac{C'_R Y_{CO_2}}{1 + s_1} \right) \qquad (4)$$

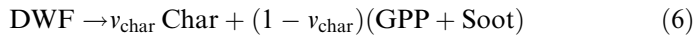where C_R and C'_R are constants taken to be 4 and 2, respectively.

The source terms for O_2 and CO_2 species equations are related to that of CO by $\dot{\omega}_{O_2} = s_1 \dot{\omega}_{CO}$ and $\dot{\omega}_{CO_2} = -(1 + s_1)\dot{\omega}_{CO}$.

If only homogeneous reactions occur above the fuel bed, both homogeneous (in the gas phase) and heterogeneous (at the surface of the solid element) chemical reactions occur in the vegetal stratum. Drying and pyrolysis of the fuel material play an essential role in the production of water vapor and combustible gases. As a consequence of pyrolysis of the wildland fuel, after drying, combustible (CO) and noncombustible (CO_2) gases, char, and soot are formed. For forest fuel matter, char consists of pure carbon (80–97%) and ash. If oxygen is present at the surface of the incandescent charreous particles, an exothermic heterogeneous global char oxidation takes place, producing CO_2 and ashes. This can be summarized by the simplified three-step mechanism

1. Endothermic drying reaction

$$WWF \rightarrow v_{H_2O} H_2O + (1 - v_{H_2O}) DWF \qquad (5)$$
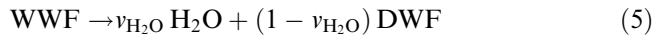
2. Endothermic global pyrolysis reaction

$$DWF \rightarrow v_{char} Char + (1 - v_{char})(GPP + Soot) \qquad (6)$$

3. Exothermic global char oxidation reaction

$$Char + sO_2 \rightarrow (1 + s - v_{ash})CO_2 + v_{ash} Ash \qquad (7)$$

where WWF and DWF symbolize wet and dry wildland fuel matter. The symbol GPP refers to gaseous pyrolysis products, with $GPP = \alpha_{CO} CO + \alpha_{CO_2} CO_2$, where α_{CO} and α_{CO_2} are the combustible and noncombustible parts of the gaseous pyrolysis products, respectively. Since the mass fraction of soot represents less than 1% of the local mass of the soot and gaseous mixture, the neglect of soot in the chemical kinetics has very little effect on the solution. That leads to $\alpha_{CO} + \alpha_{CO_2} = 1$.

The rate of each reaction above is expressed approximately by the following Arrhenius-type equations:

$$k_{H_2O} = m_{k,H_2O} A_{H_2O} T_k^{-1/2} \exp\left(\frac{-E_{H_2O}}{T_k}\right) \tag{8}$$

$$k_{pyr} = m_{k,pyr} A_{pyr} \exp\left(\frac{-E_{pyr}}{T_k}\right) \tag{9}$$

$$k_{char} = \frac{1}{s} A_{char} \alpha_k \sigma_k \rho_{O_2} \exp\left(\frac{-E_{char}}{T_k}\right)\left(1 + \beta_{char}\sqrt{Re_k}\right) \tag{10}$$

where $s = 1.65$ [16] and Re_k is the Reynolds number defined in terms of the radius of the cylindrical particle as $Re_k = 2\rho|\mathbf{u}|r_k/\mu$ with $r_k = 2/\sigma_k$. The corrective factor $1 + \beta_{char}\sqrt{Re_k}$ that appears in the reaction rate of char oxidation has been introduced to account for blowing effects on char oxidation.

Concerning the solid phase, the positions of individual fuel particles are assumed to be fixed in space. This means that, at this stage of development, our model cannot handle the dispersion of flying particles, such as burning brands which can cause spotting ahead of the fire. Using this hypothesis, the collapse of the bed after the fire's passage and its incidence on the dynamics of the flow are not taken into account. However, this simplifying hypothesis does not appear to weigh heavily when the reaction time (the time required for the flaming zone to pass a given point, and equal to the flame depth divided by the rate of spread) is low versus the time of complete combustion of the fuel particles. The bed skeleton structure is thus preserved during a certain period of time after the passage of the fire front. Particles are also assumed to be isothermal (thermally thin assumption). This assumption is reasonable for values of Biot (Bi) number less than 0.1 [17], as is the case for the range of the solid-phase parameters and fire conditions investigated.

Allowing for the assumptions previously mentioned, the governing equations for the solid phase reduce to ordinary differential equations for describing the temporal changes of the particles with respect to mass and temperature. It is worth noting that the rate of particle mass reduction relative to the thermal decomposition of the solid phase can be represented by the sum of the mass rates due to water vaporization, pyrolysis, char combustion, and ash formation. The solid-phase equations can be written as

$$\dot{m}_{k,\,H_2O} = -k_{H_2O} \tag{11}$$

$$\dot{m}_{k,\,pyr} = -k_{pyr} \tag{12}$$

$$\dot{m}_{k,\,char} = v_{char}\, k_{pyr} - k_{char} \tag{13}$$

$$\dot{m}_{k,\,ash} = v_{ash}\, k_{char} \tag{14}$$

$$\dot{m}_k = -k_{H_2O} - (1 - v_{char})\, k_{pyr} - (1 - v_{ash})\, k_{char} \tag{15}$$

$$m_k C_{pk} \frac{\partial T_k}{\partial t} = D_{\text{mass}} + Q_{rk} + Q_c \tag{16}$$

where

$$D_{\text{mass}} = -k_{\text{pyr}} L_{\text{pyr}} - \alpha_{\text{char}} k_{\text{char}} \Delta h_{\text{char}} - k_{\text{H}_2\text{O}} L_{\text{H}_2\text{O}} \tag{17}$$

and α_{char} is the fraction of the energy produced by the char combustion reaction which is deposited in the solid phase. The fraction $1 - \alpha_{\text{char}}$ is therefore deposited in the gas phase.

The source terms that appear in the gas-phase equations as a consequence of thermal degradation of the fuel material are then simply

$$S_{Y_\alpha} = \begin{cases} (1 - v_{\text{char}})\alpha_{\text{CO}} \ k_{\text{pyr}} \\ - s k_{\text{char}} \\ (1 - v_{\text{char}})\alpha_{\text{CO}_2} \ k_{\text{pyr}} + (1 + s - v_{\text{ash}}) \ k_{\text{char}} \\ k_{\text{H}_2\text{O}} \\ 0 \end{cases} \tag{18}$$

$$S_m = \sum_{\alpha=1}^{5} S_{Y_\alpha} \tag{19}$$

$$S_h = -(1 - \alpha_{\text{char}}) \ k_{\text{char}} \Delta h_{\text{char}} + \sum_{\alpha=1}^{5} S_{Y_\alpha} \ h_\alpha \tag{20}$$

In the last equation, the species enthalpy is expressed at the temperature of the solid-phase surface: $h_\alpha = h_\alpha(T_k)$.

2.1.2. Radiation transport and soot formation. For an absorbing-emitting gray particulate medium, a multiphase radiative transfer equation (MRTE) has been developed in a recent article [18]. As in the present study the vegetation stratum is composed of a single-class solid phase, the radiative intensity in the direction Ω, $I(\Omega)$, obeys the following equation:

$$\Omega_j \frac{\partial}{\partial x_j} (\alpha_g I) + (\alpha_g a_g + \alpha_k a_k) I = \alpha_g a_g I_b(T) + \alpha_k a_k I_b(T_k) \tag{21}$$

The discrete ordinates method is used for the resolution of the MRTE. This means that radiation calculations are based on solving the MRTE in $M = n(n + 2)$ discrete solutions to which a set of weights is attached. In the current study, the ordinate directions and quadratic weighting factors (μ_m, ξ_m, and w_m) were taken from the well-known TWOTRAN II code [19], and the S_8 approximation ($M = 80$) was retained. For a specific ordinate direction $m = 1, 2, \ldots, M$, defined by $\Omega_m = (\mu_m, \xi_m)$, the MRTE can be written as

$$\mu_m \frac{\partial}{\partial x} (\alpha_g I_m) + \xi_m \frac{\partial}{\partial y} (\alpha_g I_m) + (\alpha_g a_g + \alpha_k a_k) \ I_m = \alpha_g a_g I_b(T) + \alpha_k a_k I_b(T_k) \tag{22}$$

I_m is the radiative intensity in the direction Ω_m, while μ_m, ξ_m are the direction cosines with respect to the Cartesian coordinate system. This equation is integrated over a control volume. The variable-weighted scheme of Lathrop [20] is used to relate the facial intensities at the boundary of the control volume to the cell center intensity.

The divergence of the radiative heat flux, $\mathbf{q}_r$, which appears in the energy equation of the gas phase, can be expressed as

$$Q_{rg} = -\nabla.\mathbf{q}_r = \alpha_g a_g [G - 4\pi I_b(T)] \tag{23}$$

The average incident radiation defined by $G = \int_{4\pi} I(\Omega)d\Omega$ can then be approximated by $G = \sum_{m=1}^{M} w_m I_m$.

In a similar manner, the radiative source term in the energy equation of the solid phase is

$$Q_{rk} = \alpha_k a_k [G - 4\pi I_b(T_k)] \tag{24}$$

where the absorption coefficient a_k can be calculated from $a_k = A_k/4$. The calculation of the absorption coefficient as the product of the bed packing ratio, and the fuel surface area-to-volume ratio over 4 is evaluated by theory [18]. It has been also validated experimentally for excelsior and pine needle fuel arrays [21].

Following Kaplan et al. [22], the absorption coefficient of the soot/combustion products (CO_2, H_2O) mixture considered as a gray gas is evaluated from the mole fraction of the combustion products and the soot volume fraction:

$$a_g = 0.1(X_{CO_2} + X_{H_2O}) + 1,862 f_{v_s} T \tag{25}$$

Radiative exchanges between hot combustion products and the virgin combustible fuel bed is a critical aspect of flame propagation, and incandescent soot particles are the main contributors to the overhead flame radiation. The chemical nature of the burning material and local specific fire conditions (e.g., underventilation) can lead to a large production of soot. An accurate prediction of the radiative transfer requires accounting for soot production/destruction, especially in turbulent flames.

The soot model is identical to the one proposed by Kennedy et al. [23] for ethylene/air diffusion flames. Only one equation is used, namely, a transport equation for the volume fraction of soot, f_{v_s}. The three source terms in the generic form of the soot transport equation (see Table 1) account for the thermophoresis, formation, and oxidation processes, respectively.

In accordance with Grishin [12], we can assume that most of the soot in the flame is produced as a result of the pyrolysis of wildland fuels, and not from the decomposition of hydrocarbons in the gas phase. Then the source term takes the form $R_+ = v_s k_{pyr}/\rho_s$, where ρ_s is the soot density, assumed to be 1,800 kg/m^3. The latter term corresponds to the oxidation term, which is written in terms of the local oxidant concentration and the surface of soot particles. The expression of Lee et al. [24] has been used,

$$R_- = \frac{6.5 f_{v_s} p_{O_2}}{\rho_s d_s \sqrt{T}} \exp\left(\frac{-19,750}{T}\right) \tag{26}$$

where d_s is the soot particle diameter.

The observation that most sooty flames exhibit remarkably similar particle number density suggests the possibility of using an average number density in the

calculations [25]. This avoids solving an additional transport equation for the soot number density.

In the present calculations, a constant value of the particle number density is used and therefore the soot particle diameter is determined from the soot volume fraction and the number density as $d_s = (6f_{v_s}/\pi n_s)^{1/3}$.

2.1.3. Constitutive relations. The drag force per unit volume acting on the solid-phase particles can be calculated, as a first estimate, from the correlation proposed by Clift et al. [26] for spheres. As the two phases are not in local thermal equilibrium, an interfacial convective heat transfer is used to take the interaction between them into account: $Q_c = A_k h_k (T - T_k)$, where the heat transfer coefficient is expressed from the correlation of Incropera and De Witt [27] for cylinders as $h_k = 0.683\lambda \, \mathrm{Re}_k^{0.466}/2r_k$.

2.2. Numerical Procedure

The governing equations are discretized on a nonuniform grid using a finite-volume procedure along with a second-order backward Euler scheme for time integration. Diffusion terms are approximated using a second-order central difference scheme, while convective ones are discretized using a high-order upwind scheme. The ULTRASHARP approach (Universal Limiter for Tight Resolution and Accuracy with a Simple High Accuracy Resolution Program) [28] is then used. This combines the use of a high-order upwind scheme for the convective terms and a flux limiter strategy, the downwind weighting factor (DWF), to eliminate any possibility of overshoot, undershoot, or oscillation sometimes introduced by the convective schemes when the monotonicity of the solution is not ensured.

Since the transient behavior is of interest, the pressure–velocity linked equations are solved using the iterative PISO algorithm (Pressure-Implicit with Splitting of Operators) developed by Chow and Cheung [29]. The resulting systems of linear algebraic equations for each variable are then solved iteratively using a tridiagonal matrix algorithm (TDMA) [30]. In addition, to procure convergence and prevent low-frequency behavior of the solution typical of this type of buoyancy-driven flow [31], all the variables are underrelaxed using inertial relaxation [30].

Different grid sizes were tested to ensure that the numerical results were independent of the grid density. A grid size of 240×60 cells with 200×10 cells of constant size in the fuel bed was used for all of the cases solved. The time step is 0.025 s. At each time step, convergence is achieved when the maximum residual error is less than 10^{-4}.

3. MODEL RESULTS AND COMPARISON WITH EXPERIMENTAL DATA

Numerical calculations are conducted to determine the emissions of energy, gases, and soot particles from a savanna fire. Test conditions and some properties of the fuel bed used in the present work are estimated from those of experimental fires conducted in arid savanna fuels in Kruger National Park by Trollope et al. [32] and Stocks et al. [33] during the SAFARI-92 project. Since, as indicated by

the authors, fine grass is the major carrying fuel in savanna fires, the other fuel species are not considered.

The dimensions of the calculation domain are 120 m long and 60 m high. The herbaceous fuel to be burned is distributed in a 1-m-thick uniform layer from 30 to 120 m from the left boundary of the computational domain (origin of the abscissa) for a fuel loading density of 0.3922 kg/m² (3, 922 kg/ha) for Block 56 [33]. The Pretoriuskop 1400 LT weather observations on 18 September 1992 are considered, namely, a dry-bulb temperature of 303.7 K, a relative humidity of 41%, and a wind speed of 10.8 km/h at a height of approximately 1.25 m above ground level. The initial fuel moisture content is around 20% ($v_{H_2O} = 0.2$). Due to the lack of data, the surface-to-volume ratio and density of the fine fuel are estimated to 5, 000 m⁻¹ and 600 kg/m³, respectively. The specific heat of the dry fuel matter is 1, 470 J/kg K. By assuming that this value of specific heat applies to the char and ash as well, the specific heat of the solid phase is then deduced from those of water and DWF, and the mass moisture remaining in the fuel material according to

$$C_{pk} = \left(\frac{1 - m_{k, H_2O}}{m_k}\right) C_{pk}^{DWF} + \frac{m_{k,H_2O}}{m_k} C_p^{H_2O} \tag{27}$$

Due to the lack of data on forest fuels of Southern Africa, the thermokinetic constants for the drying, pyrolysis, and char combustion reactions are those given by Grishin [12] for the vegetation of Siberia: $E_{H_2O} = 5, 800$ K, $E_{pyr} = 7, 250$ K, $E_{char} = 9, 000$ K, $A_{H_2O} = 6 \times 10^5 \, s^{-1} K^{-1/2}$, $A_{pyr} = 3.63 \times 10^4 \, s^{-1}$, $A_{char} = 430$ m/s, $v_{char} = 0.3$, $v_s = 0.03$, $v_{ash} = 0.1$ (3% of DWF), and $\alpha_{CO} = 0.8$. The energy generated by the oxidation of char is deposited equally in both phases ($\alpha_{char} = 0.5$) and $\beta_{char} = 0.2$. The char oxidation reaction is an exothermic process with $\Delta h_{char} = -12 \times 10^6$ J/kg, while pyrolysis is assumed to be slightly endothermic, with $L_{pyr} = 418$ J/kg. To describe the dynamics of spreading fires in Southern Africa on a quantitative level, it is necessary to determine thermokinetic constants for the vegetation of the Southern Africa. This can be achieved from specific experimental data by solving the inverse kinetic problem as was done by Grishin [12] and more recently by Grishin et al. [34] for the process of drying of forest fuels of Siberia.

At the upstream boundary, the incoming air flow is taken as that corresponding to the atmospheric surface layer over a uniform, flat terrain. Assuming neutral stratification of the atmosphere, air flow properties depend on height y, surface roughness y_0, turbulent friction velocity u^*, and Monin-Obukhov length according to [35]

$$u = 2.5u^* \ln\left(\frac{y}{y_0}\right) \qquad k = \frac{u^{*2}}{\sqrt{C_\mu}} \qquad \varepsilon = \frac{2.5u^{*3}}{y} \tag{28}$$

with

$$u^* = \frac{u_H}{2.5 \ln(H/y_0)} \tag{29}$$

and $y_0 = 3.8 \times 10^{-5}$ m. In this equation, u_H is the known mean wind speed at a height H, and u is the desired wind speed at some other height y.

3.1. Pyrolysis Front Trajectory and Fuel Consumption Ratio

Figure 2 shows the predicted trajectories of the pyrolysis front $x_{pyr}(t)$. The pyrolysis front location may be defined as the rightmost position where the solid-phase temperature exceeds 500 K, which is found by Albini [36] to be representative of the onset of flaming combustion. Anyway, the steady propagation rate is roughly the same if a higher solid-phase temperature is considered.

Although the code is used in its time-dependent mode, a genuine steady state is obtained with a steady firespread rate of 0.614 m/s. This value is very close to that observed for KNP fires, where the average head fire spread rate is 0.63 m/s for block 56 [33].

The time evolution of the fuel consumption ratio (FCR), determined as the ratio of mass of burned solid fuel (initial fuel mass − current fuel mass) to the initial mass of fuel placed on a virtual weighting platform located between $x = 50$ m and $x = 55$ m, is also reported in Figure 2. The computed FCR is 89.3%, while that determined from the experiments is about 91.5% (3, 588 kg/ha) for block 56. Thus the comparison indicates that the FCR deduced from the rates of particle mass reduction (due to the thermal decomposition of the fuel material) using first-order Arrhenius laws compares well with the available experimental data. Although this close agreement does not prove the validity of the proposed kinetic model, it does justify using it for wildfire modeling.
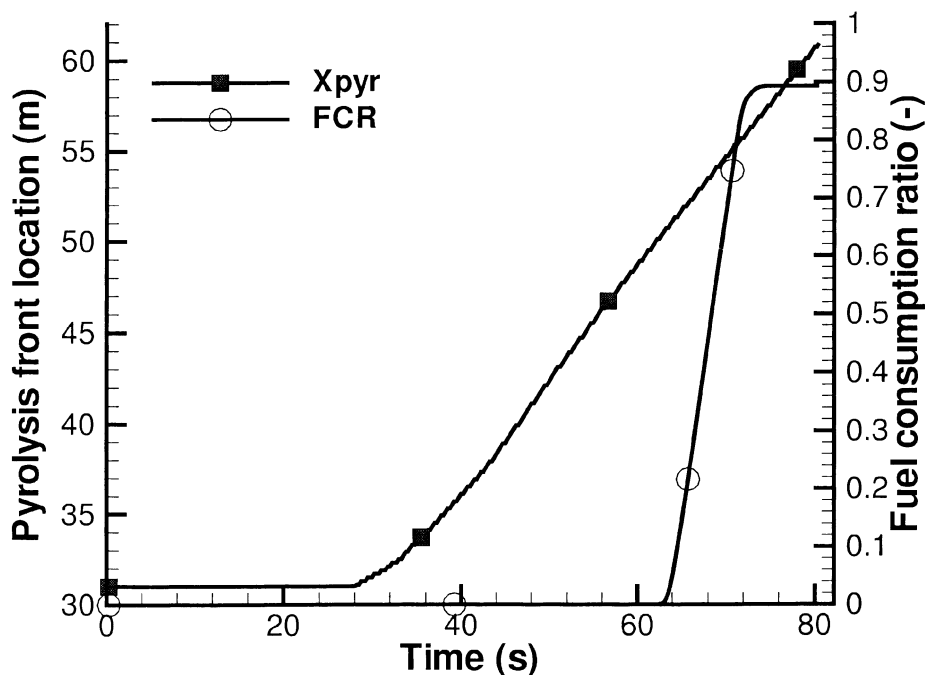

Figure 2. Pyrolysis front history and time evolution of the consumption ratio of a fuel sample located between $x = 50$ m and $x = 55$ m.

3.2. Flame Geometry and Fire Plume Properties

The geometry of the flame is generally studied through the parameters of height, length, and angle of deflection of the flame. As pointed out by Zukoski [37], eye-averaged and video pictures depend on the light from the flame itself and record the radiation emitted by burning soot particles. Hence, the flame height data concern that part of the combustion zone made visible by radiation from burning soot. As a temperature of 823 K is sometimes used to define the average flame height [37], the same criterion is used here to outline the visible flame surface.

The time evolution of the uppermost location of isotherm 823 K is plotted in Figure 3. From $t = 56$ s, the flame height remains approximatively constant with time and equal to 200 cm. Figure 4 shows steady-state isocontours of gas temperature and vorticity, along with velocity vectors. In experiments, flame length is calculated from the measured average flame height using the flame tilt obtained from visual observation of low-level aerial photographs [33]. Using this method, flame length on block 56 ranged from 173 to 230 cm. As indicated by the authors, it is worth noting that flame heights were very variable in block 56 $(2-346$ cm$)$, with an average value of 169 cm. When comparing these experimental values to the computed geometric characteristics of the flame shown in Figure 4, the results obtained by our 2-D model shows a slight overattachment of the flame on the fuel bed compared to experiments. According to Zukoski [37], this disagreement may be due to
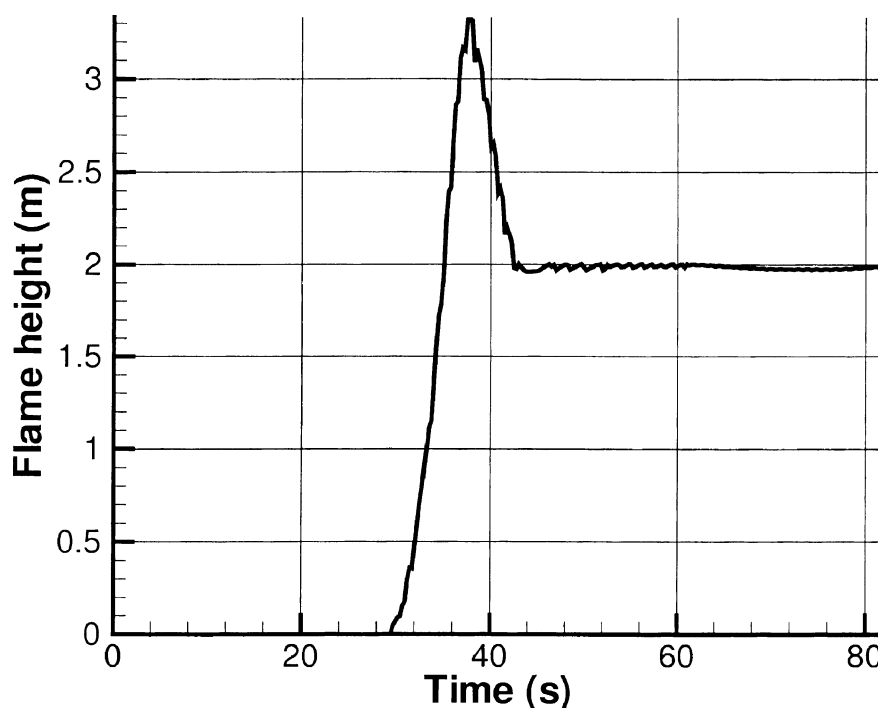

Figure 3. Time evolution of the flame height defined as the uppermost location of isotherm 823 K.

(a) Gas temperature (K)

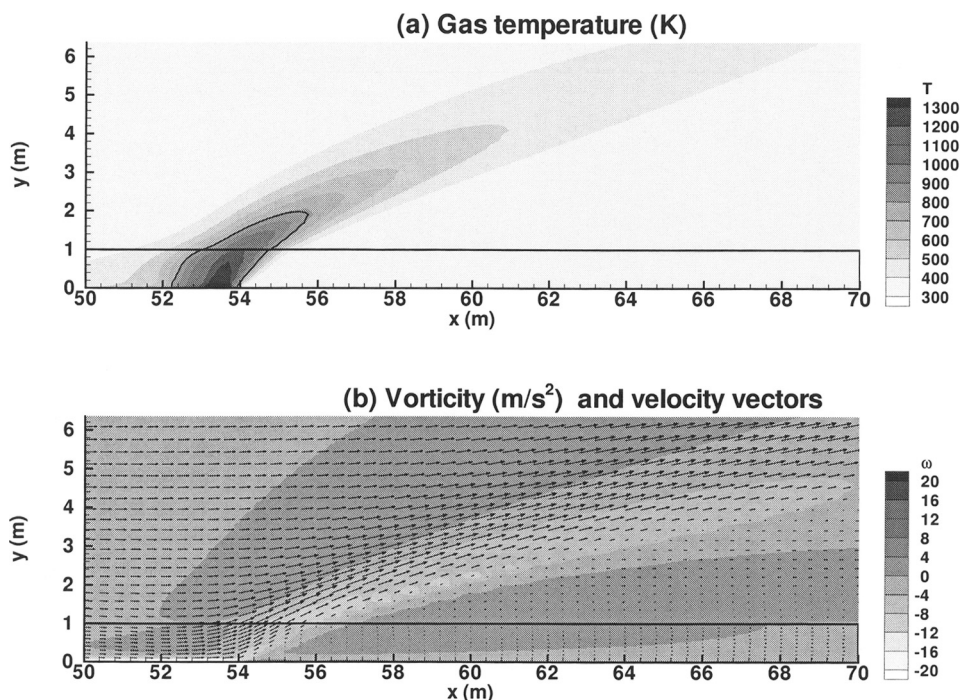## (b) Vorticity (m/s²) and velocity vectors

Figure 4. Steady-state isocontours of the gas temperature and vorticity, and velocity vectors. The location of the isotherm 823 K, as an indicator of the average flame surface, is represented by the solid line.

the fact that the attachment is more pronounced in 2-D than in 3-D flows due to the absence of cross flow.

A closer view of the computed isocontours of temperature for both phases, magnitude of radiative heat flux, species mass fraction, and soot volume fraction is shown in Figure 5. The solid line superimposed on the contours shows the location of the flame surface. The region in the flame where the gas temperature is maximum is the core of the flame, while the maximum in the solid-phase temperature is observed within the char combustion zone. In the char combustion region, heterogeneous reaction occurs between char and oxygen, leading to oxygen depletion and carbon dioxyde formation. For the wind velocity considered, the low fuel loading density ($\alpha_k = 5.45 \times 10^{-4}$) causes continuous oxygenation of the combustion zone, as confirmed by examination of Figures 4b and 5e. This contributes to a high rate of spread of savanna fires under drought conditions. After passing through the entire combustion zone, the side flow deviates upward.

As a result of the thermal degradation of the fuel, the maximum mass fractions of CO and H_2O, and soot volume fraction are located in the region of intense pyrolysis within the flame (Figures 5d, 5g, and 5h). The sooting region is located in the fuel bed along the leeward side of the flame surface, where the soot volume fraction reaches a maximum value of 1.2×10^6; then, it gradually decreases at higher positions by an oxidation process.
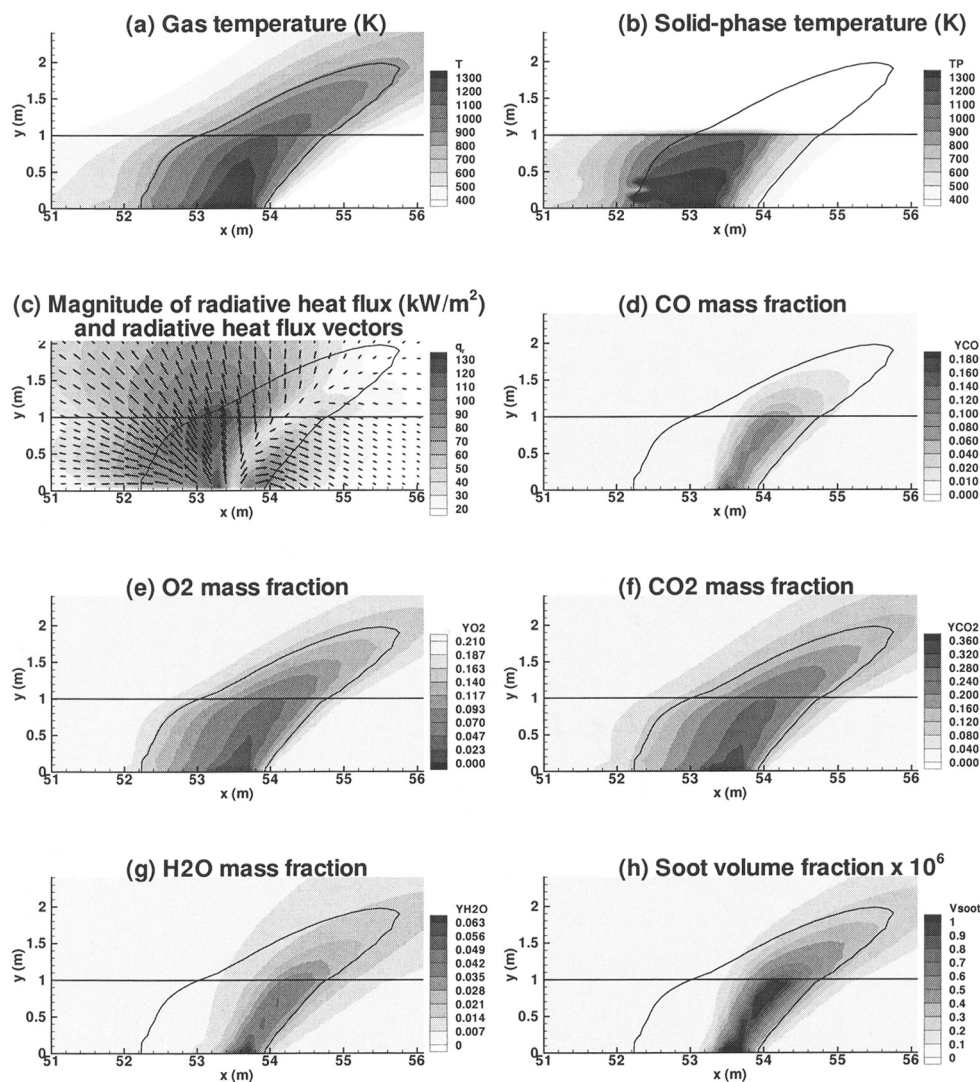
Figure 5. Steady-state isocontours of the fire plume properties and solid-phase temperature in the fuel bed. The location of the isotherm 823 K, as an indicator of the average flame surface, is represented by the solid line.

Figure 5c also shows the radiative flux vectors and isocontours of the magnitude of the radiative heat flux, defined as $(q_{rx}^2 + q_{ry}^2)^{1/2}$. The length of each of the radiative flux vectors is proportional to its magnitude. A comparative examination of Figures 5c and 5h reveals the strong attenuation of radiation in the heavily sooting region. The largest flux vectors are located behind the sooting region. This is due not to the soot particles contribution, as its concentration is low, but to that of the high-temperature solid phase. Most of the radiation is emitted backwards.
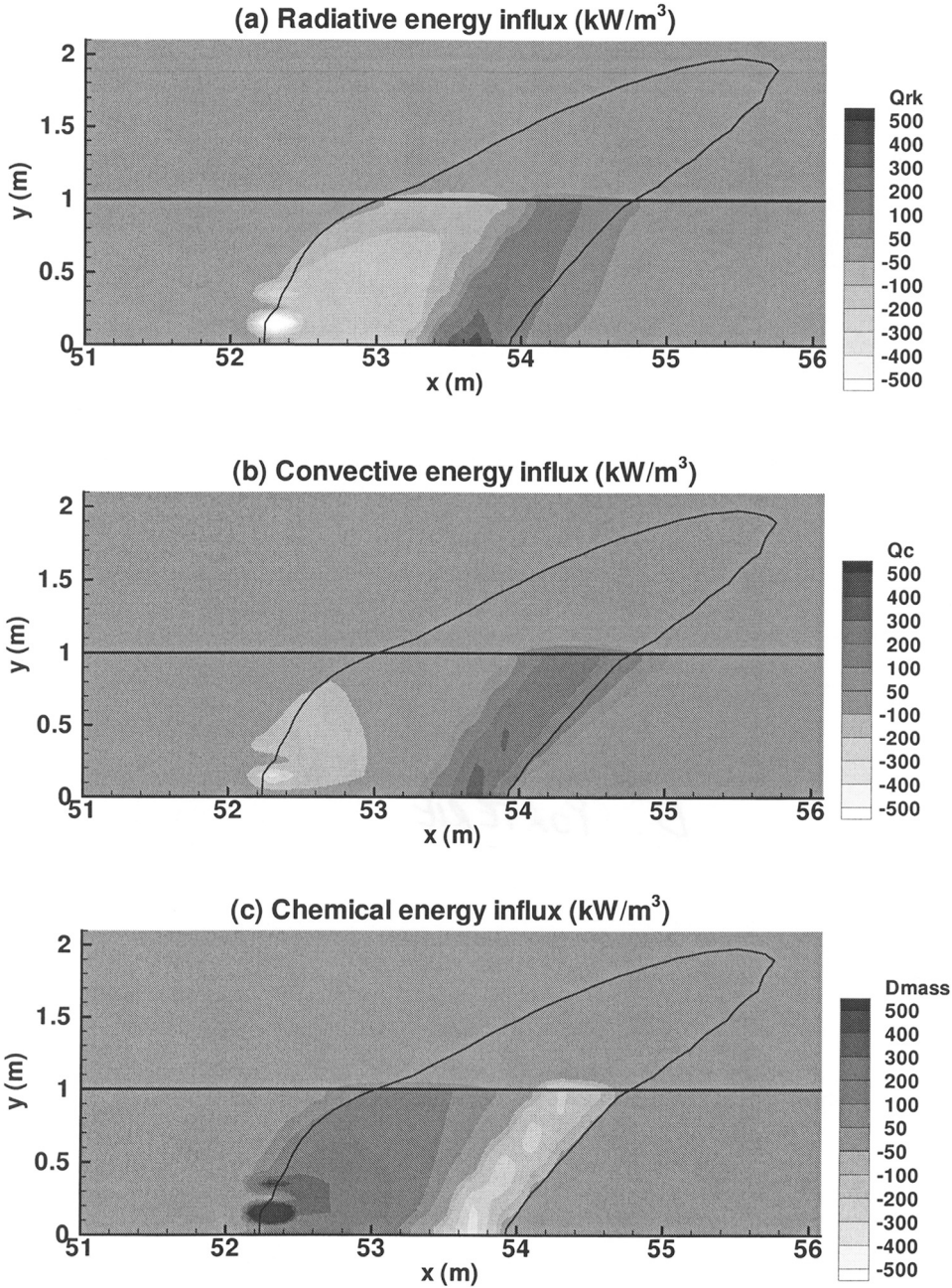
Figure 6. Comparison of the energy influxes from the combustion zone to the unburned fuel. The location of the isotherm 823 K, as an indicator of the average flame surface, is represented by the solid line.

3.3. Rate-Controlling Heat Transfer Mechanisms

The rate of spread is controlled by the rate of energy transfer from the burning zone to the unburned solid material. An analysis which quantifies the energy-transfer mechanisms is available from the present model. This can be done by comparing the contribution of each source term of the solid-phase energy equation.

Figure 6 shows the contours of the radiative (Q_r), convective (Q_c), and chemical (D_{mass}) energy influxes; the former includes radiation from both the flame and solid phase, the latter is relative to the thermal decomposition of the solid fuel. According to the conclusions of Pagni and Peterson [7] for the intermediate convective velocity considered in the present application, the dominant preheating mechanism is convection, with a moderate contribution from radiation. In the present configuration, the overhead flame radiation is not dominant, and since the depth of the fuel bed is of the same order as the mean free path of radiation, i.e., $\delta_k = 1/a_k = 0.576$ m, the depth of the fuel bed is almost fully involved in the radiative heating process. This partly explains why the isocontours of the radiative heat flux are nearly vertical in the pyrolysis region (Figure 6a) and the radiative contribution to the heating of adjacent unburned fuel elements is moderate.

The region of maximum chemical energy influx is located behind the burning zone (Figure 6c), which corresponds to the char combustion zone. Char combustion increases the solid-phase temperature, which in turn enhances the energy losses due to radiation (Figure 6a). This chemical heat contribution is minimum near the fire front as a result of the endothermic water vaporization and pyrolysis processes (Figure 6c). The convective cooling, i.e., the cooling effect of fresh air coming from the left, is clearly visible in Figure 6b at the rear of the combustion zone.

3.4. Fire Emissions

A good description of the fire emissions can be obtained from the consecutive vertical distributions of the area-integrated gas temperature, species mass fraction, and soot volume fraction, as shown in Figure 7. The maximum computed values of CO, CO_2, and H_2O mass fraction and soot volume fraction occur mainly at the top of the litter ($y = 1$ m), with the exception of the O_2 mass fraction, which is minimum. This is due to the competitive effects of homogeneous and heterogeneous chemical reactions and intense pyrolysis in the fuel bed. Because of the high oxygen concentration above the fuel bed, a rapid decrease in CO mass fraction is observed in Figure 7b. At a height of about 3 m, the fuel depletion is complete.

The predicted peak soot volume fraction is about 3.5×10^{-7}, which corresponds to a mean soot particle diameter $d_s = 0.51$ μm. Leaving the flaming zone, the mean diameter of the soot particles is 0.34 μm. This is in accordance with Doppler lidar and Doppler radar observations within the fire plume [38].

An overall description can be easily obtained by characterizing the fire source as a source of heat and radiation. By way of example, the fire considered can be described by a 3-m^2 source at a mean temperature of 1, 100 K (Figure 8). Applying the same averaging procedure to all variables allows a very convenient approximation of the fire region.
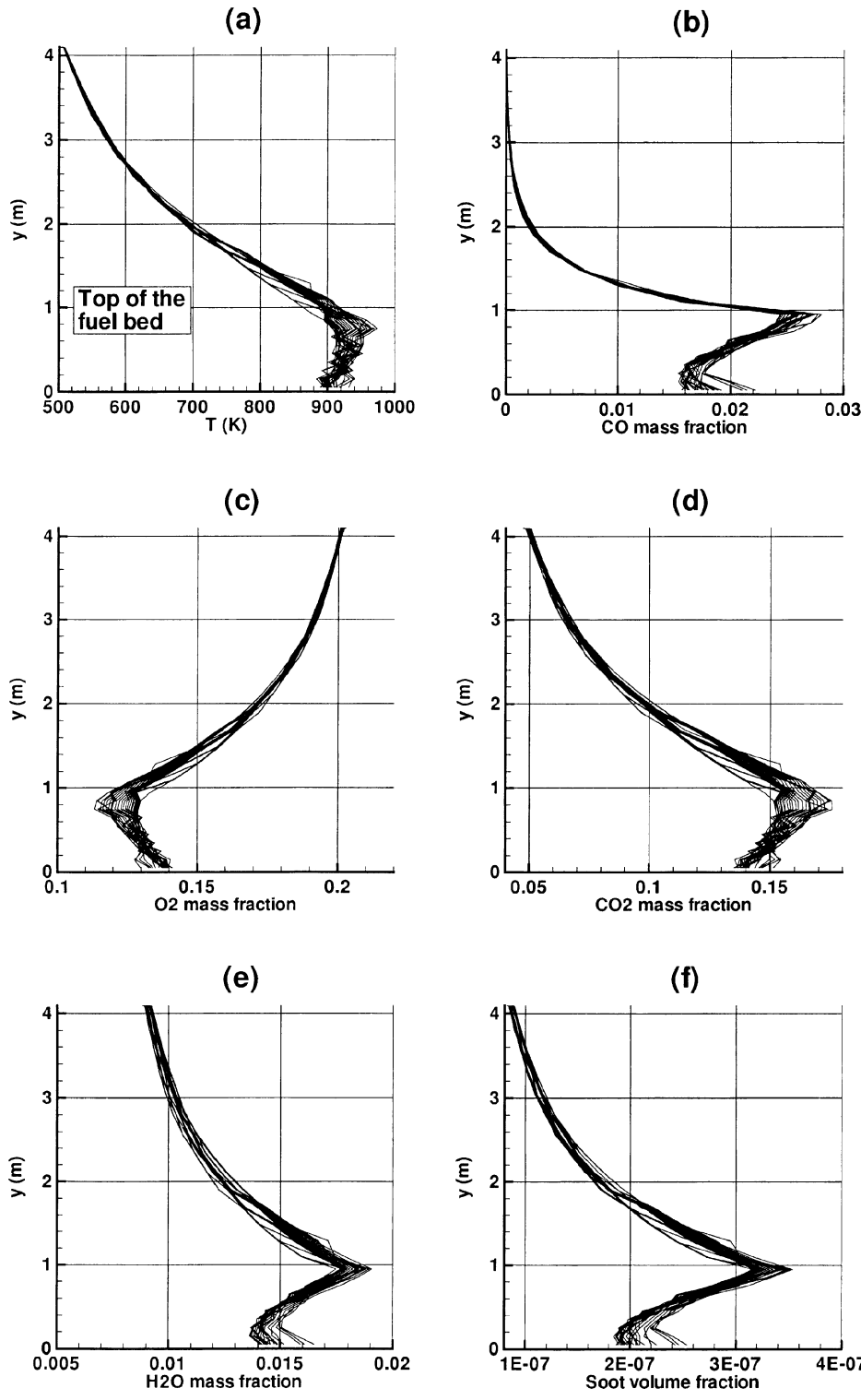
(a)

(b)

(c)

(d)

(e)

(f)

Figure 7. Successive area-integrated gas temperature, CO, O_2, CO_2, and H_2O mass fractions, and soot volume fraction as a function of height.
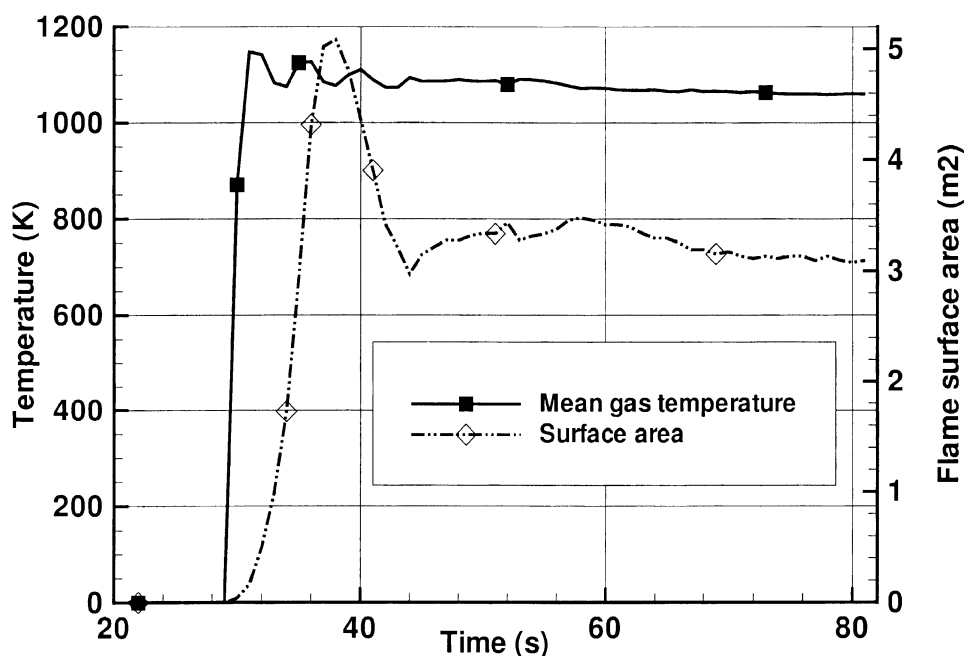
Figure 8. Time evolution of the gas temperature averaged over the flame surface and flame surface area.

4. CONCLUSIONS

This investigation has demonstrated the suitability of a fine-scale model for describing the processes that take place in the near-field of a vegetation fire. It provides temporal and spatial distributions of the fire emissions, namely, those of soot, energy, and gaseous species. This emissions information could be used to represent the fire as input data or source terms (at prescribed locations of the physical domain) in atmospheric models as well as radiative sources for fire detection and monitoring. Where comparisons with experimental data have been possible, the predictions give reasonable agreement with those data. The model was able to accurately predict the rate of spread and fuel consumption ratio of an experimental fire conducted in KNP savanna. It is encouraging to note that predictions indicate correct trends in flame geometry.

REFERENCES

1. P. J. Crutzen and G. R. Carmichael, Modeling the Influence of Fires on Atmospheric Chemistry, in P. J. Crutzen and J. G. Goldammer (eds.), *Fire in the Environment: The Ecological, Atmospheric, and Climatic Importance of Vegetation Fires*, pp. 89–103, Wiley, New York, 1993.
2. J. Trentmann, M. O. Andreae, H. F. Graf, P. V. Hobbs, R. D. Ottmar, and T. Trautmann, Simulation of a Biomass Burning Plume: Comparison of Model Results with Observation, *J. Geophys. Res.*, vol. 107, 10.1029/2001JD000410, 2002.

3. A. M. Grishin, B. G. Voronin, A. A. Dolgov, and V. S. Sofronov, Determining the Forest Fuel Combustion Product Emission, in A. M. Grishin (ed.), *Conjugate Problems of Mechanics and Ecology*, pp. 88–96, Pub. House Tomsk University, Tomsk, Russia, 1992.

4. A. M. Grishin, A. A. Dolgov, and A. F. Tsimbalyuk, A Method of Determining and Calculating the Ejections of the Polluting Substances from the Forest Fires, The State Committee of the Russian Federation on Environmental Protection. An Official Edition, Moscow, Russia, 1997.

5. M. O. Andreae, Biomass Burning: its History, Use, and Distribution and its Impact on Environmental Quality and Global Climate, in J. S. Levine (ed.), *Global Biomass Burning: Atmospheric, Climatic, and Biospheric Implications*, pp. 3–21, MIT Press, Cambridge, MA, 1991.

6. B. Porterie, D. Morvan, J. C. Loraud, and M. Larini, Firespread through Fuel Beds: Modeling of Wind–Aided Fires and Induced Hydrodynamics, *Phys. Fluids*, vol. 12, pp. 1762–1782, 2000.

7. P. J. Pagni and T. G. Peterson, Flame Spread through Porous Fuels, *Proc. 14th Symp. (Int.) on Combustion*, pp. 1099–1107, The Combustion Institute, Pittsburgh, PA, 1973.

8. L. O. Bellemare, B. Porterie, and J. C. Loraud, On the Prediction of Firebreak Efficiency, *Combustion Sci. Technol.*, vol. 163, pp. 131–176, 2001.

9. B. Porterie, J. C. Loraud, L. O. Bellemare, and J. L. Consalvi, A Physically–Based Modeling of the Onset of Crowning, *Combustion Sci. Technol.*, vol. 175, pp. 1–33, 2003.

10. R. O. Weber, Modelling Fire Spread through Fuel Beds, *Prog. Energy Combustion Sci.*, vol. 17, pp. 67–82, 1991.

11. A. M. Grishin, Mathematical Modeling of Forest Fires, *Novosibirsk Institute of Theoretical and Applied Mechanics of Siberian Branch of the Academy of Sciences of the USSR*, vol. 9, no. 4, pp. 30–56, 1978.

12. A. M. Grishin, *Mathematical Modeling of Forest Fires, and New Methods of Fighting Them*, Pub. House Tomsk University, Tomsk, Russia, 1992.

13. A. M. Grishin, General Mathematical Model of the Forest and Peat Fires, *Achieve. Mech.*, vol. 1, pp. 41–89, 2002.

14. V. Yakhot and M. Smith, The Renormalization Group, the ε-Expansion and Derivation of Turbulence Models, *J. Sci. Comput.*, vol. 7, pp. 35–61, 1992.

15. B. F. Magnussen and B. H. Hjertager, On Mathematical Modeling of Turbulent Combustion with Special Emphasis on Soot Formation and Combustion, *Proc. 16th Symp. (Int.) on Combustion*, pp. 719–729, The Combustion Institute, Pittsburgh, PA, 1976.

16. T. Kashiwagi and H. Nambu, Global Kinetics Constants for Thermal Oxidative Degradation of a Cellulosic Paper, *Combustion & Flame*, vol. 88, pp. 345–368, 1992.

17. J. F. Sacadura, *Initiation aux transferts thermiques*, 4th ed., Technique et Documentation, Paris, 1993.

18. J. L. Consalvi, B. Porterie, and J. C. Loraud, Model of Radiative Heat Transfer in Particulate Media, *Int. J. Heat Mass Transfer*, vol. 45, pp. 2755–2768, 2002.

19. K. D. Lathrop and F. W. Brinkley, TWOTRAN–II: An Interfaced, Exportable Version of the TWOTRAN Code for Two–Dimensional Transport, Rep. LA–4848–MS, Los Alamos Natl. Lab., Los Alamos, NM, 1973.

20. K. D. Lathrop, Spatial Differencing of the Transport Equation: Positivity vs. Accuracy, *J. Comput. Phys.*, vol. 4, pp. 475–498, 1969.

21. B. W. Butler, Experimental Measurements of Radiant Heat Fluxes from Simulated Wildfire Flames, *Proc. 12th Conf. on Fire and Forest Meteorology*, Jekyll Island, GA, 1993.

22. C. R. Kaplan, C. R. Shaddix, and K. C. Smyth, Computations of Enhanced Soot Production in Time–Varying CH_4/Air Diffusion Flames, *Combustion & Flame*, vol. 106, pp. 392–405, 1996.

23. I. M. Kennedy, W. Kollmann, and J. Y. Chen, A Model for Soot Formation in a Laminar Diffusion Flame, *Combustion & Flame*, vol. 81, pp. 73–85, 1990.

24. K. B. Lee, M. W. Thring, and J. M. Beer, On the Rate of Combustion of Soot in a Laminar Soot Flame, *Combustion & Flame*, vol. 6, pp. 137–145, 1962.

25. W. Kollmann, I. M. Kennedy, M. Metternich, and J. Y. Chen, Application of a Soot Model to a Turbulent Ethylene Diffusion Flame, in H. Bockhorn (ed.), *Soot Formation in Combustion*, pp. 503–526, Springer-Verlag, Berlin, 1994.

26. R. Clift, J. R. Grace, and M. E. Weber, *Bubbles, Drops and Particles*, Academic, New York, 1978.

27. F. P. Incropera and D. P. De Witt, *Fundamentals of Heat and Mass Transfer*, Wiley, New York, 1985.

28. B. P. Leonard and J. E. Drummond, Why You Should Not Use Hybrid, Power–Law or Related Exponential Schemes for Convective Modelling. There are Much Better Alternatives, *Int. J. Numer. Meth. Eng.*, vol. 20, pp. 421–442, 1995.

29. W. K. Chow and Y. L. Cheung, Comparison of the Algorithms PISO and SIMPLER for Solving Pressure–Velocity Linked Equations in Simulating Compartment Fire, *Numer. Heat Transfer A*, vol. 31, pp. 87–112, 1997.

30. S. V. Patankar, *Numerical Heat Transfer and Fluid Flow*, McGraw-Hill, New York, 1980.

31. J. B. Moss, Turbulent Diffusion Flames, in G. Cox (ed.), *Combustion Fundamentals of Fire*, pp. 221–272, Academic, San Diego, CA, 1995.

32. W. S. W. Trollope, L. A. Trollope, A. L. F. Potgieter, and N. Zambatis, SAFARI-92 Characterization of Biomass and Fire Behavior in the Small Experimental Burns in the Kruger National Park, *J. Geophys. Res.*, vol. 101, pp. 23531–23539, 1996.

33. B. J. Stocks, V. B. Wan Wilgen, W. S. W. Trollope, D. J. McRae, A. Mason, F. Weirich, and A. L. F. Potgieter, Fuels and Fire Behavior Dynamics on Large–Scale Savanna Fires in Kruger National Park, South Africa, *J. Geophys. Res.*, vol. 101, pp. 23541–23550, 1996.

34. A. M. Grishin, A. Y. Kuzin, and E. N. Alexeyenko, Determination of Kinetic Characteristics of the Process of Drying of Forest Combustibles, *J. Eng. Phys. Thermophys.*, vol. 76, pp. 170–175, 2003.

35. P. Panofsky and J. Dutton, *Atmospheric Turbulence*, Wiley, New York, 1984.

36. F. A. Albini, A Model for the Wind-Blown Flame from a Line Fire, *Combustion & Flame*, vol. 43, pp. 155–174, 1981.

37. E. E. Zukoski, Properties of Fire Plumes, in G. Cox (ed.), *Combustion Fundamentals of Fire*, pp. 101–219, Academic, San Diego, CA, 1995.

38. R. M. Banta, L. D. Olivier, E. T. Holloway, R. A. Kropfli, B. W. Bartram, R. E. Cupp, and M. J. Post, Smoke–Column Observations from Two Forest Fires Using Doppler Lidar and Doppler Radar, *J. Appl. Meteorol.*, vol. 31, pp. 1328–1348, 1995.